Nonmonotonic spatial structure of interneuronal correlations in prefrontal microcircuits

Shervin Safavi[a,b,1], Abhilash Dwarakanath[a,1], Vishal Kapoor[a,b], Joachim Werner[a], Nicholas G. Hatsopoulos[c], Nikos K. Logothetis[a,d,2], and Theofanis I. Panagiotaropoulos[a,e,2]

[a]Department Physiology of Cognitive Processes, Max Planck Institute for Biological Cybernetics, 72076 Tübingen, Germany; [b]International Max Planck Research School for Cognitive and Systems Neuroscience, University of Tübingen, 72074 Tübingen, Germany; [c]Department of Organismal Biology and Anatomy, University of Chicago, Chicago, IL 60637; [d]Division of Imaging Science and Biomedical Engineering, University of Manchester, 72074 Manchester, United Kingdom; and [e]Cognitive Neuroimaging Unit, Commissariat à l'Énergie Atomique, Division Sciences de la Vie (DSV), Institut d'imagerie Biomédicale (I2BM), INSERM, Université Paris-Sud, Université Paris-Saclay, Neurospin Center, 91191 Gif/Yvette, France

Correlated fluctuations of single neuron discharges, on a mesoscopic scale, decrease as a function of lateral distance in early sensory cortices, reflecting a rapid spatial decay of lateral connection probability and excitation. However, spatial periodicities in horizontal connectivity and associational input as well as an enhanced probability of lateral excitatory connections in the association cortex could theoretically result in nonmonotonic correlation structures. Here, we show such a spatially nonmonotonic correlation structure, characterized by significantly positive long-range correlations, in the inferior convexity of the macaque prefrontal cortex. This functional connectivity kernel was more pronounced during wakefulness than anesthesia and could be largely attributed to the spatial pattern of correlated variability between functionally similar neurons during structured visual stimulation. These results suggest that the spatial decay of lateral functional connectivity is not a common organizational principle of neocortical microcircuits. A nonmonotonic correlation structure could reflect a critical topological feature of prefrontal microcircuits, facilitating their role in integrative processes.

functional connectivity | prefrontal cortex | network structure | long-range interactions | noise correlations

The intraareal connectivity patterns of neural populations in the mammalian neocortex frequently repeat across cortical areas (1–4). Such canonical rules with general validity are important in understanding basic organizational principles and ensemble computations in cortical networks (1–3, 5). Nevertheless, identifying deviations from these rules between sensory and higher-order, association cortical areas could reveal properties leading to cortical network specialization and higher cognitive functions (1–3, 5, 6).

The spatial structure of intraareal functional connectivity is frequently inferred by measuring the trial-by-trial correlated variability of neuronal discharges (spike count correlations) (7). One of the most well-established properties (a canonical feature) of intraareal, mesoscopic, functional connectivity is a so-called limited-range correlation structure, reflecting a monotonic decrease of spike count correlations as a function of spatial distance and tuning similarity (7–17). However, this distance-dependent decrease of correlations has been almost exclusively derived from recordings in primary sensory cortical areas or inferred from recordings in the prefrontal cortex (PFC) with various constraints like a rather limited scale (18) (see also *Discussion*). As a result, it is currently unclear whether known differences in the structure of anatomical connectivity across the cortical hierarchy could also give rise to different spatial patterns of functional connectivity (19–22).

Specifically, the rapid spatial decay of correlations in sensory cortex is widely assumed to reflect a similar rapid decay in lateral anatomical connectivity and excitation (23). In early visual cortical areas, correlations rapidly decrease as a function of distance (refs. 12, 14, and 17; but also see refs. 24 and 25) in a manner that closely reflects anatomical findings about the limited spread

and density of intrinsic lateral connections (19, 26–29). However, lateral connections are significantly expanded in later stages of the cortical hierarchy, like the PFC (19, 21, 28–31). In this higher-order association area, lateral connections commonly extend to distances up to 7–8 mm (28, 29, 31), while patches of connected populations are both larger and more distant from each other compared with sensory cortex (29, 32). Although horizontal axons in macaque V1 can extend up to 4 mm, they do not form clear patches, and for distances of 2–3 mm laterally to the injection patch border, only a small number of cells are labeled in comparison with higher-order areas (19, 27, 29, 33, 34). In addition to the more extended intrinsic lateral connectivity, associational input from other cortical areas to the PFC also forms stripes with an average distance of 1.5 mm and contributes to the spatial periodicities in lateral organization (35). Finally, the proportion of lateral excitatory connections is higher in the PFC (95%) compared with V1 (75%) (36).

Whether these significant differences in the structural architecture of the PFC compared with early sensory areas also result in a distinct spatial pattern of functional connectivity is currently unknown. Intuitively, higher probability of long-range lateral excitatory connections and stripe-like associational input patterns could give rise to strong spike count correlations across local and spatially remote populations, with weaker correlations for populations

Significance

The spatial structure of correlated activity of neurons in lower-order visual areas has been shown to linearly decrease as a measure of distance. The shape of correlated variability is a defining feature of cortical microcircuits, as it constrains the computational power and diversity of a region. We show here a nonmonotonic spatial structure of functional connectivity in the prefrontal cortex (PFC) where distal interactions are just as strong as proximal interactions during visual engagement of functionally similar PFC neurons. Such a nonmonotonic structure of functional connectivity could have far-reaching consequences in rethinking the nature and role of prefrontal microcircuits in various cognitive states.

NEUROSCIENCE

in intermediate distances. To address this question, we recorded simultaneously the activity of large neural populations in the inferior convexity of the macaque PFC during both anesthetized and awake states using multielectrode Utah arrays (37). In both anesthetized and awake states, the spatial pattern of pairwise correlated variability was nonmonotonic with significantly positive long-range correlations. A major source of nonmonotonicity could be attributed to the spatial pattern of correlated variability between functionally similar neurons.

Results

We used multielectrode Utah arrays (4 × 4 mm, 10 × 10 electrodes, interelectrode distance 400 μm, electrode length 1 mm; Fig. 1*A*) to record spiking activity from the inferior convexity of the ventrolateral PFC (vlPFC) during repeated visual stimulation with movie clips in two anesthetized macaque monkeys (Fig. 1*B*) and with sinusoidal gratings, drifting in eight different directions, in two awake behaving macaques (Fig. 1*C*). To evaluate the effect of structured visual input on correlated variability, we contrasted periods of visual stimulation to intertrial as well as spontaneous activity (long periods of neural activity without any task demands). Both anesthetized- and awake-state recordings resulted in the simultaneous monitoring of multiple, well-isolated single units that remained stable for several hours of recording (Fig. 1*D*). On average, in each dataset, we recorded from 103 ± 16 (mean $\pm$ SEM) single units and $5,305 \pm 1,681$ pairs during anesthesia (Fig. S1*A*)

and 107 ± 14 single units and $5,758 \pm 1,675$ pairs during wakefulness (Fig. S1*B*).

Spatial Structure of Correlated Variability During Anesthesia and Wakefulness. It has been repeatedly shown that correlated variability of spike counts in early sensory, especially visual, areas in different species decreases as a function of lateral distance, with strong interactions for proximal and progressively weaker interactions for distal (up to 4 mm) neurons (14, 15, 17). We investigated the same relationship between spike count correlations (r_{sc}) and lateral distance up to 4 mm in the vlPFC.

Visual stimulation with movie clips during anesthesia or with drifting gratings during wakefulness gave rise to a spatial pattern in the structure of correlated variability that was fundamentally different compared with early sensory areas: strong and positive long-range (>2.5 mm) correlations that were comparable to the average magnitude of local (up to 1 mm) correlations and significantly weaker correlations for intermediate distances (red curves in Fig. 2 and Fig. S1 *A* and *B*).

We evaluated the statistical significance of nonmonotonicity and long-range correlations by comparing the distributions of pairwise correlations in populations recorded from nearby (0.5 mm for anesthetized and 1 mm for awake), intermediate (2.5 mm), and distant (3.5–4 mm) sites during visual stimulation. The choice of these particular distance bins was based on the local extrema of correlated variability as a function of distance

Fig. 1. Implantation, visual stimulation, and quality of single unit isolation. (*A*) Location of the implanted array with respect to arcuate and principal sulci and an example of typical waveforms acquired across the implanted cortical patch during a typical recording session in an awake animal. (*B*) Anesthetized visual stimulation protocol: 10 s of movie clip presentation was interleaved with 10-s-long intertrial (stimulus off) periods for 200 repetitions. (*C*) Awake visual stimulation protocol: The macaques initiated each trial by fixating on a red dot for 300 ms, following which a drifting sinusoidal grating was presented monocular for 1,000 ms. After 1,000 ms of visual stimulation and a 300-ms stimulus-off period, liquid reward was delivered for successful fixation throughout the trial period. An intertrial period of 1,000 ms preceded the next trial. Each block of trials comprised eight different motion directions (exemplified by differently colored arrows) presented in a random order. (*D*) Single unit isolation quality: Each column shows the activity recorded from four channels recorded in two different datasets, one from each of the two monkeys (monkeys H and A). The 500 example waveforms for single units (shown as colored clusters) and noise spikes (multiunit activity shown as gray clusters) along with the mean waveform in dashed white, and their corresponding first and second principal components (pc1 and pc2) are shown in the first and second row, respectively. In the last row, the first principal component of all of the waveforms in a cluster is plotted over time, demonstrating stability of recordings and single unit isolation for periods lasting ~3.5–4 h. amp, amplitude.
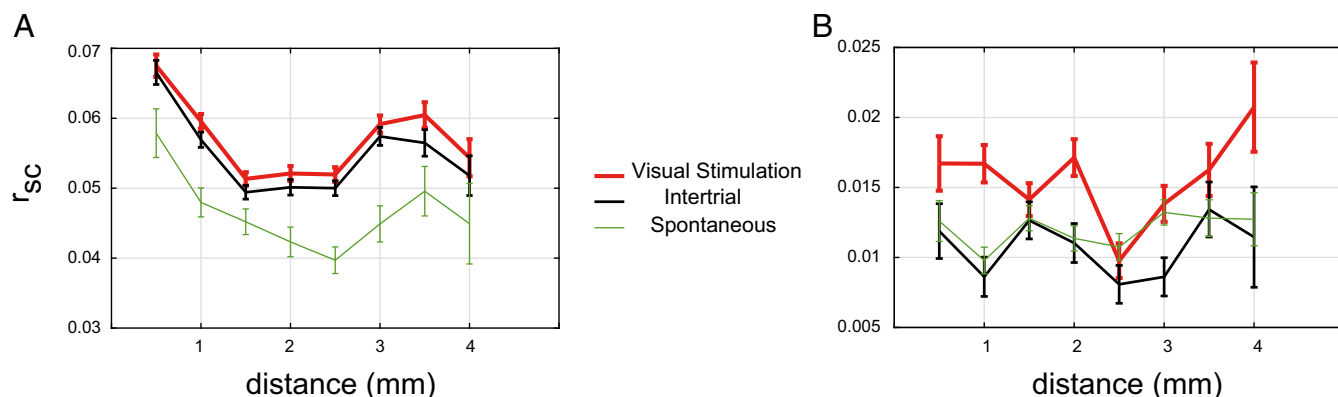
Fig. 2. Spatial structure of correlated variability. (*A*) Spike count correlations (r_{sc}) during visual stimulation (red), intertrial (black), and spontaneous activity (green) as a function of lateral spatial distance (millimeters) between cell pairs for anesthetized-state recordings (error bars represent mean ± SEM). (*B*) Same as *A* for awake-state recordings.

during visual stimulation. For all of the comparisons made across these distance bins, to assess the significance of the differences in correlated variability, we used the Wilcoxon rank-sum test (unless otherwise mentioned explicitly). Moreover, as we made the comparisons across the three key distance bins, we assessed the significance after a Bonferroni correction for multiple comparisons (corrected $P = 0.0167$). Summary statistics of Bonferroni-corrected P values are available in Tables S1–S3 (for anesthetized and awake data).

Average correlated variability between neurons located in intermediate distances was significantly lower compared with very proximal neurons in the anesthetized ($\overline{r_{sc}}^{0.5\ mm} = 0.0675 \pm 0.0016$ vs. $\overline{r_{sc}}^{2.5\ mm} = 0.0520 \pm 0.0010$; $P < 10^{-10}$; Fig. 2*A*, red curve, and Fig. S2*A*) state. In the awake recordings, correlations among nearby neurons, i.e., at a pairwise distance of 1 mm, showed a significant difference from those at the local minimum of the spatial correlation structure ($\overline{r_{sc}}^{1\ mm} = 0.0167 \pm 0.0013$ vs. $\overline{r_{sc}}^{2.5\ mm} = 0.0098 \pm 0.0012$; $P = 0.0038$; Fig. 2*B*, red curve, and Fig. S2*D*). Following this minimum, correlations during anesthesia significantly increased from 2.5 to 3 mm ($\overline{r_{sc}}^{2.5\ mm} = 0.0520 \pm 0.0010$ vs. $\overline{r_{sc}}^{3\ mm} = 0.0592 \pm 0.0012$; $P = 0.012$) and 3.5 mm ($\overline{r_{sc}}^{3.5\ mm} = 0.0605 \pm 0.0018$; $P = 0.0040$). A similar increase in correlated variability for progressively more distant populations was also observed in the awake state, where correlations significantly increased from 2.5 mm to both 3.5 mm ($\overline{r_{sc}}^{2.5\ mm} = 0.0098 \pm 0.0012$ vs. $\overline{r_{sc}}^{3.5\ mm} = 0.0163 \pm 0.0019$; $P = 0.0076$) and 4 mm ($\overline{r_{sc}}^{2.5\ mm} = 0.0098 \pm 0.0012$ vs. $\overline{r_{sc}}^{4\ mm} = 0.0207 \pm 0.0032$; $P = 0.0079$).

In the awake-state recordings, the average magnitude of correlations for distant populations, located 3.5–4 mm apart, was not different from the respective magnitude for nearby pairs ($\overline{r_{sc}}^{1\ mm} = 0.0167 \pm 0.0013$ vs. $\overline{r_{sc}}^{3.5\ mm} = 0.0163 \pm 0.0019$, $P = 0.7$; and $\overline{r_{sc}}^{4\ mm} = 0.0207 \pm 0.0032$, $P = 0.3$; Fig. 2*B*, red curve, and Fig. S2*D*). In addition, both local and distant average correlations were significantly positive ($P < 0.005$, t test). However, in the anesthetized recordings, despite the significant increase of correlations for distant neurons compared with intermediate distances, long-range correlations remained significantly lower compared with nearby neurons ($\overline{r_{sc}}^{0.5\ mm} = 0.075 \pm 0.0016$ vs. $\overline{r_{sc}}^{3.5\ mm} = 0.0605 \pm 0.0018$, $P = 0.0056$; and $\overline{r_{sc}}^{4\ mm} = 0.0544 \pm 0.0027$, $P = 0.0008$; Fig. 2*A*, red curve, and Fig. S2*A*), suggesting that anesthesia-induced fluctuations had a nonhomogeneous impact on the spatial structure of correlations. Such nonhomogeneous, state-dependent weighting on the spatial structure of correlations has been reported in previous studies of primary visual cortex as well (12).

The nonmonotonic structure in correlated variability could not be ascribed to random spatial variability in firing rates, since it could be observed even when correlated variability was estimated for populations with matched geometric mean firing rates across lateral distances (Fig. S3). Furthermore, to confirm that the intrinsic nonuniformity of spatial sampling with Utah arrays did

not lead to the nonmonotonic structure of correlated variability, we used a bootstrapping analysis of our spatial sampling (Fig. S4). This analysis showed that equalized resampling of pairs across distance bins also resulted in a nonmonotonic correlated variability structure (Fig. 2).

The decrease in correlations from nearby neuronal pairs (0.5 mm in the anesthetized state and 1 mm in the awake state) to 2.5 mm and the increase from 2.5 to 3.5 or 4 mm was observed in both the anesthetized and awake states. However, in the awake-state recordings, we also observed an additional pronounced peak at 2 mm (Fig. 2*B* and Fig. S2*D*). Lack of this peak at intermediate distances in our anesthetized recordings is compatible with other studies performed during anesthesia and provides further evidence for a nonhomogeneous, state-dependent weighting on the spatial structure of correlated variability (12, 14, 17, 25). These common features in the spatial structure of correlated activity across anesthetized ($\overline{r_{sc}}^{anesth}$) and awake ($\overline{r_{sc}}^{awake}$) states were observed despite significant differences in the average magnitude of correlations [$\overline{r_{sc}}^{anesth} = 0.0574 \pm 3 \times 10^{-4}$ (mean ± SEM) vs. $\overline{r_{sc}}^{awake} = 0.0153 \pm 3 \times 10^{-4}$; $P = 0$; Fig. 3*A*]. Despite being very close to zero, average correlations during visual stimulation were significantly positive during the awake state ($P < 10^{-104}$; t test).

Visual Stimulation Shapes the Spatial Structure of Correlated Variability. We evaluated the impact of structured visual stimulation on the spatial pattern of correlated variability by comparing correlations during visual stimulation with movie clips (during anesthesia) or drifting sinusoidal gratings (during wakefulness) to the respective pattern during intertrial and spontaneous activity periods. Compared with periods of intertrial activity, visual stimulation resulted in a significant increase of correlated variability in both anesthetized recordings ($\overline{r_{sc}}$ visual $= 0.0574 \pm 3 \times 10^{-4}$ vs. $\overline{r_{sc}}$ intertrial $= 0.0554 \pm 3 \times 10^{-4}$; $P < 10^{-3}$; Fig. 3*B*) and awake recordings ($\overline{r_{sc}}$ visual $= 0.0153 \pm 3 \times 10^{-4}$ vs. $\overline{r_{sc}}$ intertrial $= 0.011 \pm 4 \times 10^{-4}$; $P = 6.7 \times 10^{-5}$; Fig. 3*C*).

Visual stimulation in the awake state significantly shaped a spatially inhomogeneous, nonmonotonic structure of correlated variability. In striking contrast to the significant differences observed for the same lateral distances during visual stimulation, we found that correlations during the intertrial period were not different between local and intermediate populations ($\overline{r_{sc}}^{0.5\ mm} = 0.0119 \pm 0.0020$ vs. $\overline{r_{sc}}^{2.5\ mm} = 0.0081 \pm 0.0014$, $P > 0.3$; Fig. 2*B*, black curve, and Fig. S2*B*) or intermediate and distant populations ($\overline{r_{sc}}^{2.5\ mm} = 0.0081 \pm 0.0014$ vs. $\overline{r_{sc}}^{3.5\ mm} = 0.0134 \pm 0.0020$, $P = 0.08$; and vs. $\overline{r_{sc}}^{4\ mm} = 0.0115 \pm 0.0036$, $P > 0.25$; Fig. 2*B*, black curve, and Fig. S2*B*). Spatially homogeneous correlations were also observed during periods without any structured visual input or task engagement, in data collected during spontaneous activity (Fig. 2*B*, green curve). In these epochs, we also found no difference between local and intermediate correlations ($\overline{r_{sc}}^{0.5\ mm} = 0.0126 \pm 0.0015$ vs. $\overline{r_{sc}}^{2.5\ mm} = 0.0107 \pm 9.5 \times 10^{-4}$;
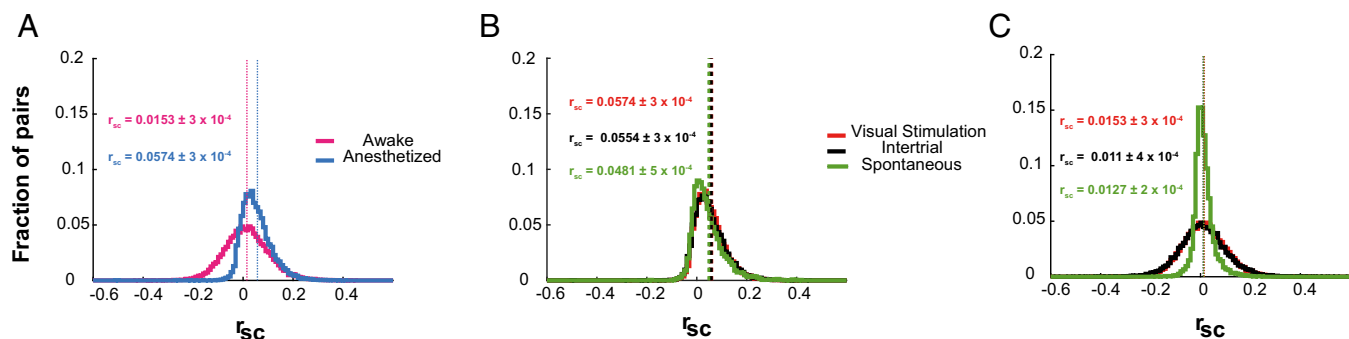
Fig. 3. Distributions of correlated variability across different states and conditions. (*A*) Distribution of pairwise correlated variability (fraction of pairs) and mean values (dotted lines) during visual stimulation for anesthetized (blue) and awake (pink) recordings. Correlated variability was significantly stronger during anesthesia as a result of a shift in the distribution of pairwise correlations toward positive values. (*B*) Same as *A* for anesthetized-state recordings during visual stimulation (red), intertrial (black), and spontaneous activity (green) periods. (*C*) Same as *B* for awake-state recordings.

$P = 0.6$) and very similar correlations between intermediate and distant populations ($\overline{r_{sc}}^{2.5\ mm} = 0.0107 \pm 9.5 \times 10^{-4}$ vs. $\overline{r_{sc}}^{3.5\ mm} = 0.0128 \pm 0.0013$, $P > 0.9$; vs. $\overline{r_{sc}}^{4\ mm} = 0.0127 \pm 0.0019$, $P > 0.17$; Fig. 2*B*, green curve).

We quantified the magnitude of spatial inhomogeneity in the structure of correlations across different conditions and states (*Experimental Procedures*). A clear difference in the rate of changes in correlated variability was observed in awake-state recordings (Fig. 4*A*), where visual stimulation resulted in the strongest spatial variability and intertrial activity in the weakest (almost constant average correlation as a function of lateral distance). A similar spatial variability was also observed under anesthesia (Fig. 4*B*); however, the average rate of change was comparable across the two conditions of visual stimulation and intertrial, but different during spontaneous activity. The difference in the structure of functional connectivity between visual stimulation and intertrial periods across anesthesia and awake states could be attributed to the lack of saccadic eye movements in intertrial periods during anesthesia. Saccadic eye movements reset visual perception (38), and their absence could create a persistent network state, showing no reset, resulting in very similar patterns of correlations during visual stimulation and intertrial periods.

These results suggest that the spatial structure of correlated variability in the PFC is inhomogeneous. The magnitude of inhomogeneity depended not only on the variation of global states such as wakefulness or anesthesia, but most importantly on behavioral demands, i.e., visual stimulation, intertrial (anticipation of the succeeding trial), or spontaneous activity (no behavioral load). Although traces of inhomogeneity in the spatial structure of correlations were observed during spontaneous activity or intertrial periods, structured visual stimulation during the awake state appeared to result in the strongest spatial inhomogeneity in the correlation structure.

Prevalence of Nonmonotonic Spatial Structure in Functionally Similar Populations. Lateral connectivity in PFC has been hypothesized to preferentially target neurons with functional similarities (e.g., similar spatial tuning), similar to iso-orientation columns in the visual cortex [Goldman-Rakic (39)]. Therefore, we next examined whether the source of the nonmonotonic correlated variability could be traced to populations of neurons that were modulated similarly by visual input. First, tuning functions for each recorded unit were obtained based on the discharge response to sinusoidal gratings drifting in eight different directions (Fig. 5). The correlation between tuning functions (signal correlation; r_{signal}) provided a measure of functional similarity among the recorded pairs (see *Experimental Procedures* for more details). We analyzed the relationship between the spatial structure of functional connectivity and functional similarity of pairwise responses (i.e., signal correlations). The relationship between signal correlations, noise correlations, and interneuronal

distance (Fig. 6*A*) points to a stronger nonmonotonic trend for pairs with positive signal correlations.

Specifically, we computed the noise correlation across distance bins for pairs with positive signal correlations ($0.1 < r_{signal} < 0.9$) during visual stimulation (Fig. 6 *A* and *B*). A nonmonotonic trend could be observed; however, the differences between the first local maximum to the local minimum, and the local minimum to the next local maximum were marginally significant ($\overline{r_{sc}}^{0.5\ mm} = 0.0266 \pm 0.0032$ vs. $\overline{r_{sc}}^{2.5\ mm} = 0.0165 \pm 0.0021$, $P = 0.07$; and $\overline{r_{sc}}^{2.5\ mm} = 0.0165 \pm 0.0021$ vs. $\overline{r_{sc}}^{4\ mm} = 0.0266 \pm 0.0054$, $P = 0.1$; green curve in Fig. 6*B*). The nonmonotonic trend was also confirmed from fitting first- and second-degree polynomials to these data. The adjusted-R^2 goodness-of-fit measure for a line (first-degree polynomial, monotonic) was −0.15, whereas the same measure for a quadratic function (second-degree polynomial, the simplest nonmonotonic function) (40) yielded a value of 0.3, pointing to the quadratic curve being a much better fit to the data (Fig. 7*A*). Progressively higher thresholds for signal correlation, resulting in sampling populations with stronger functional similarity, did not qualitatively change these effects that were characterized by a significant decrease in intermediate distance (∼2.5 mm) correlations (Fig. S5 *B*, *E*, and *H*).

During intertrial periods, correlated variability of the same population of functionally similar neurons (functional similarity estimated during the visual stimulation period) was homogenous (Fig. 6 *C* and *D*). For positive signal correlations ($0.1 < r_{signal} < 0.9$) during visual stimulation, the strength of correlated variability between nearby and intermediate neurons was not significantly different ($\overline{r_{sc}}^{0.5\ mm} = 0.015 \pm 0.0033$ vs. $\overline{r_{sc}}^{2.5\ mm} = 0.0111 \pm 0.0022$, $P = 0.3$; and $\overline{r_{sc}}^{1\ mm} = 0.008 \pm 0.0023$ vs. $\overline{r_{sc}}^{2.5\ mm} = 0.0111 \pm 0.0022$, $P = 0.9$;
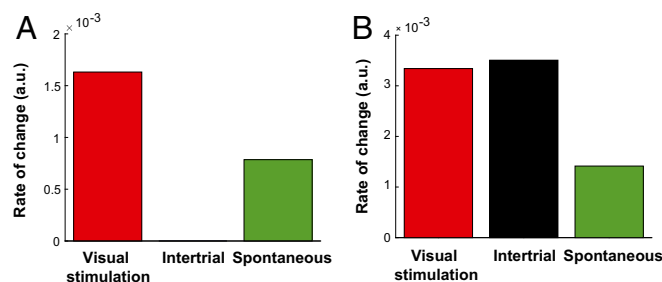
Fig. 4. Quantification of spatial inhomogeneity in the structure of correlated variability. (*A*) Spatial inhomogeneity in the structure of correlations across different conditions during awake-state recordings. Spatial inhomogeneity was quantified by computing the average of the absolute rate of change in the correlation structure across successive distance bins (only those rates significantly different in successive distance bins; see also *Experimental Procedures*). (*B*) Same as *A* for anesthetized-state recordings.

Fig. 5. Visual modulation of single unit activity during wakefulness. Spike raster plots and overlaid peristimulus time histograms (PSTHs) for four single units across all eight orientations (0–315°) are shown. Polar plots for each unit show the preferred direction(s) of motion. The green lines in the center indicate the resultant length and direction (see *SI Experimental Procedures* for more details). *A* and *B* are typical examples of bimodally tuned prefrontal units with significant responses for opposite directions of motion (orientation-selective responses). *C* and *D* are examples of sharper, unimodal responses for a particular direction of motion.

green curve in Fig. 6*D*), and correlations between neurons in intermediate and distant locations were also very similar ($\overline{r_{sc}}^{2.5\ mm} = 0.0111 \pm 0.0022$ vs. $\overline{r_{sc}}^{3.5\ mm} = 0.0077 \pm 0.0034$, $P = 0.8$; and vs. $\overline{r_{sc}}^{4\ mm} = 0.0057 \pm 0.0068$, $P = 0.9$). A similar fitting procedure as used for the data in the visual-stimulation period was also used to test for the observed trends in the intertrial period. Fitting a line yielded an adjusted R^2 value of 0.48, whereas fitting a quadratic function yielded an adjusted R^2 value of 0.5, pointing to both fits being quantitatively similar (Fig. 7*B*). However, whereas the quadratic fit in the visual-stimulation period yielded a U-shaped curve that clearly displayed the equivalence between local and distant populations, this equivalence was not seen during the intertrial period, where distant populations were weakly correlated compared with local populations.

Furthermore, when local (0.5–1 mm) and distant (3.5–4 mm) populations were pooled at a spatial resolution of 1 mm, a clear and specific strengthening of correlated variability at the flanks was observed during structured visual stimulation epochs ($P^{0.5-1\ mm}_{VisStim\ vs.\ Intertrial} = 0.00024$; $P^{3.5-4\ mm}_{VisStim\ vs.\ Intertrial} = 0.017$; $P^{2.5}_{VisStim\ vs.\ Intertrial} = 0.14$). Together, the nonmonotonic spatial structure of functionally similar populations during visual stimulation was stronger compared with the more homogeneous structure (Fig. 7*B*) of the same population during the intertrial period, pointing to a role of structured visual input in shaping the nonmonotonic structure of correlated variability in functionally similar populations.

When the same fitting procedure as described above was performed on pairs of functionally dissimilar neurons (i.e., $-0.9 <$ $r_{signal} < -0.1$), a linearly increasing trend provided a slightly better fit compared with a quadratic fit (adjusted R^2 linear = 0.33; adjusted R^2 quadratic = 0.2). However, when local and distant populations were binned as for the high-signal correlation pairs, correlated variability in the flanks during visual stimulation and intertrial was identical ($P^{0.5-1\ mm}_{VisStim\ vs.\ Intertrial} = 0.64$; $P^{3.5-4\ mm}_{VisStim\ vs.\ Intertrial} = 0.7$). Examples of pairwise neuronal responses from neurons with similar signal correlations and sampled from short, intermediate, and long lateral distances are presented in Fig. 6 *E–G*.

Several factors changed between the anesthetized vs. awake animal experiments. For instance, recordings were performed in different monkeys, using different stimuli (movie clips vs. moving grating) and different data-acquisition systems and spike extraction methods. Despite these differences, interneuronal correlations showed a similar spatial structure in both anesthetized and awake recordings with visual stimulation. More specifically, these results suggest that spatial inhomogeneities in the functional architecture of the PFC arise from strong local and long-range lateral functional interactions between functionally similar neurons, which are particularly pronounced during structured visual stimulation in the awake state.

Discussion

Spatial Structure of Prefrontal Correlated Variability and Relationship to Anatomical Structure. Spatial decay in the strength of spike count correlations on a mesoscopic scale, up to 4 mm of lateral

Fig. 6. Effect of functional similarity on the spatial structure of correlated variability. (*A*) Correlated variability as a function of distance and signal correlation for the pooled data recorded during visual stimulation in the awake state. The color of each pixel indicates the average correlated variability for pairs that their signal correlation and distance landed in the specific bin. Pixels containing <10 pairs were removed (white pixels). Correlated variability values are indicated by the color bar at the right of the image. Data were smoothed with a 2D Gaussian (SD of 1 bin) for display purposes. (*B*) Correlated variability as a function of distance (similar to Fig. 2) among neuronal pairs with signal correlation >0.1 and <0.9, i.e., the nonzero upper part of matrix represented in *A* with green line; and among pairs with signal correlation higher than −0.9 and less than −0.1, i.e., the nonzero lower part of matrix represented in *A* with blue line (mean ± SEM as error bars). (*C* and *D*) Same as *A* and *B* for the intertrial period. The signal correlation matrix is computed from the visual stimulation period, and the correlated variability of these populations in the intertrial period is mapped onto the pixels in *C*. (*E–G*) Three example pairs with high signal correlations and high, low, and high correlated variability from the nearest, the intermediate, and the farthest distance bins, respectively. The polar plot shows the vector sum of the tuning for each neuron in a given pair, while the scatter plots depict their z-score normalized responses. Example raster plots are overlaid with the PSTHs for the preferred direction of motion. Despite the sparseness in firing for some of the neurons, sharp tunings can be observed (compare raster plots with polar plots).

Fig. 7. Fitting trends to the relationship between noise correlations and distance for functionally similar populations. (*A*) Linear ($y = ax + b$) and quadratic ($y = ax^2 + bx + c$) trends fit to noise correlations as a function of distance for functionally similar neurons ($0.1 < r_{signal} < 0.9$) during visual stimulation periods. A negative adjusted R^2 value for the linear fit and a positive R^2 value of 0.3 for the quadratic fit clearly demonstrate a nonmonotonic trend being shaped by visual stimulation. A positive symmetric convexity also points toward a strengthening of local and long-range connectivity during visual stimulation. (*B*) Linear ($y = ax + b$) and quadratic ($y = ax^2 + bx + c$) trends fit to noise correlations as a function of distance for functionally similar neurons ($0.1 < r_{signal} < 0.9$) during intertrial periods. Very similar R^2 values for both the fits (linear = 0.48 and quadratic = 0.5) demonstrate that the quadratic trend is not much different from a linearly decreasing trend. Moreover, the asymmetric negative convexity of the quadratic curve points to a lack of strengthening of local and long-range correlations when no visual stimulation is present. (*C*) Linear ($y = ax + b$) and quadratic ($y = ax^2 + bx + c$) trends fit to noise correlations as a function of distance for functionally dissimilar neurons ($-0.9 < r_{signal} < -0.1$) during visual stimulation periods. The fitting results display a monotonically increasing trend of noise correlations as a function of distance. These pairs of neurons do not display the characteristic positive convexity shown by functionally similar neurons where local and distant populations have equivalent correlated variability, pointing to a different mechanism of functional connectivity driving this relationship.

distance, is largely considered a canonical feature of functional connectivity. Our results suggest that this spatial decay is not observed in the PFC, since nearby and distant neurons are correlated to the same degree, thus reflecting a fundamentally different lateral functional connectivity structure compared with primary sensory areas like V1 (14, 17, 24, 25). Such a functional connectivity pattern is likely to directly reflect the underlying anatomical organization of prefrontal neural populations into spatially distributed clusters connected through local and long-range excitatory collaterals (28, 32, 36). Indeed, in awake-state recordings, the spatially inhomogeneous correlation pattern reflected bumps of ~1.5- to 2-mm width (Fig. 2*B*), which closely matches the spatial distribution (~1.5 mm maximum width) of laterally labeled stripes of neuronal assemblies in supragranular prefrontal layers [Kritzer and Goldman-Rakic (28) and Pucak et al. (32)].

Although purely anatomical methods cannot identify functional similarities across connected populations (and vice versa), an influential hypothesis of structural connectivity in the PFC assumes that long-range excitatory collaterals target clusters of neurons with similar functional preference, like spatial tuning (39). Our results provide experimental evidence supporting this hypothesis, since correlated variability of functionally similar neurons was a major source of spatial inhomogeneities, on a spatial scale that closely matches the anatomical estimates of periodicities in lateral connections and associational input. In contrast, functionally dissimilar neurons showed a strengthening of correlated variability across distance, but did not display any clear periodicity. Interestingly, despite a columnar structure of orientation preference in V1 [Hubel et al. (41)], correlated variability was significantly lower for distant populations, potentially reflecting a much weaker influence of lateral connections. Although a definite answer to the exact relationship between structural and functional connectivity in the PFC could be provided in the future from functional anatomy techniques, the spatial scale consistency across anatomical and functional connectivity measures seems to suggest that, indeed, structural connectivity is likely to cluster functionally similar prefrontal populations into local and distant functionally connected ensembles.

The spatial pattern of horizontal connections could be one likely source of the nonmonotonic correlation structure in PFC. Another source could be ascribed to spatially distributed input from associational or thalamic areas to the PFC (35, 42, 43).

Regardless of the underlying mechanism, the impact of spatially clustered, similarly tuned, correlated prefrontal neurons to distant cortical and subcortical targets may facilitate the role of PFC in large-scale transmission and integration of information. Specifically, such prefrontal clusters could be thought of as separate channels of information that project to distant cortical and subcortical areas (42, 43). Correlated prefrontal output could coordinate these distant targets and therefore contribute to large-scale information processing.

Spatial Structure of Prefrontal Correlated Variability and Integrative Processing. PFC is a central subnetwork playing a crucial role in cognitive computations due to an increase in the integrative aspect of information processing in higher-order cortical areas (44, 45). This progressive increase in integrative functions across the cortical hierarchy was recently suggested to be mediated by a similar hierarchy in the timescales of intrinsic fluctuations that arise due to systematic changes in the anatomical structure, like heterogeneous connectivity of local circuitry (6, 46, 47). A nonmonotonic spatial structure of correlated variability differentiates prefrontal functional connectivity from primary sensory areas and could therefore be relevant to the emergence of prefrontal-specific timescales (6, 46–48). Network topology was recently suggested to affect timescales since physical distance between connected nodes was shown to increase as timescale lengthened (49).

From a graph-theoretical perspective, a spatially inhomogeneous connectivity profile, combining strong local and long-range functional connectivity, similar to what we observed in the PFC for functionally similar populations, could reflect a network with shorter average path length and higher average clustering coefficient compared with a network with monotonically decreasing correlations and/or uncorrelated long-range functional connectivity (like V1) (50). These topological features are known to facilitate efficient integrative processing (51, 52) and could reflect a fundamental characteristic of laterally organized prefrontal microcircuits compared with primary visual cortex, where, despite positive local correlations, long-range activity on the same spatial scale is uncorrelated (25).

Some recent findings shed light on the spatial functional organization of prefrontal populations that could be critical for integrative processing (53–55). Kiani et al. (54) revealed a natural grouping of prefrontal neurons into isolated clusters that remained stable across various conditions (e.g., different epochs

of task, spontaneous activity), therefore suggesting that intrinsic lateral connections play a prominent role in shaping functional parcellation in PFC. In another study, Markowitz et al. (55) found that different working memory stages are implemented in the PFC by spatially and functionally segregated subnetworks. More importantly, the spiking activity of these subnetworks during working memory is coordinated, indicating a distributed network that integrates different aspects of working memory through long-range interactions. Our findings, revealing spatially distributed clusters of correlated neurons with similar feature selectivity, provide further evidence for the existence and function of long-range functional interactions within the PFC, which seems to be instrumental for higher-order integrative processing.

Comparison with Previous Studies of Correlated Variability in the PFC. Experimental constraints prevented previous studies in dorsolateral areas of the PFC, around the principal sulcus, from capturing a nonmonotonic correlation structure (9, 56, 57). These studies were constrained by a maximum interelectrode distance of 1 mm, and our findings up to this distance were indeed consistent, showing a decrease in correlations up to 1 mm.

A number of other factors might also have prevented previous studies that used Utah arrays in other areas of the PFC to capture the nonmonotonic spatial structure of correlations that we report here. First, it is likely that the nonmonotonic structure is specific for this particular region of PFC, i.e., vlPFC, since none of these studies involved recordings in the vlPFC, but rather in area 8A (i.e., the frontal eye fields) (54, 58). The source of this region-specific discrepancy between our results and previous studies (54, 58) could be potentially traced to differences in the involvement of various prefrontal regions in visual processing. For example, the probability of finding feature-selective neurons (e.g., direction selective neurons) may be higher in the vlPFC compared with area 8A [Hussar and Pasternak (59)]. Since our data validated the spatially nonmonotonic correlation structure during visual stimulation with movie clips and direction of motion, the lack of a similar spatial structure in the frontal eye fields could be due to its differential functional role.

Leavitt et al. (58) recorded using 4×4-mm Utah arrays in area 8A and found a monotonically decreasing correlation structure. However, hardware limitations allowed them to record simultaneously from blocks of only 32 electrodes each time, limiting the spatial coverage that would prevent an extensive examination of the potential spatial anisotropy in area 8A. Kiani et al. (54), using the same electrode arrays, recorded simultaneously from all 96 electrodes and also reported a monotonic decrease of correlations for multiunit activity for distances up to 4 mm. However, the length of electrodes was 1.5 mm, compared with the 1-mm length used in our recordings. Therefore, the monotonically decreasing correlations might be due to layer-specific effects as reported in primary visual cortex (60, 61).

Comparison with Previous Studies of Correlated Variability in Primary Visual Cortex. Rosenbaum et al. (25) recently provided evidence for a nonmonotonic correlation structure in superficial layers (L2/3) of primary visual cortex without strong long-range correlations. In particular, they reanalyzed data collected with Utah arrays during anesthesia and, only after removing the effect of latent shared variability, found that nearby neurons were weakly but significantly correlated, neurons at intermediate distances were negatively correlated, and distant neurons were uncorrelated (r_{sc} not different from 0).

There are some major differences between this study and our results from prefrontal recordings on the same spatial scale. First, the average correlation coefficient for distant (3–4 mm apart) neurons in these V1 recordings was not different from zero, which implies an absence of correlation rather than weak correlation between distant populations. In striking contrast, the average magnitude of long-range correlations for the same distance in the awake PFC recordings was (*i*) significantly positive and (*ii*) comparable to the magnitude of correlations for nearby

neurons. This suggests that long-range (3–4 mm) functional connectivity in PFC is stronger and in fact results in significant long-range correlations compared with the primary visual cortex, where, despite a weak nonmonotonicity, the average correlated variability between distant neurons is not different from zero. The second, and more important, difference pertains to the conditions under which the nonmonotonic structure was detectable. The Rosenbaum et al. (25) results in V1 suggested an underlying nonmonotonic functional connectivity that was washed out by the strong modulatory effects of global state fluctuations (e.g., up and down states) observed during anesthesia in macaques (12) and in rodents during anesthesia and quiet wakefulness (62, 63). Specifically, the nonmonotonic correlation structure was revealed only after removing the effect of global latent fluctuations via Gaussian process factor analysis (GPFA). This suggests that a nonmonotonic structure in the primary visual cortex should be directly detectable in data recorded from awake animals where the anesthesia-induced global fluctuations are absent. However, to the best of our knowledge, until now there has been no direct experimental evidence in awake V1 recordings. In contrast, Ecker et al. (24) found a flat correlation structure in awake V1 recordings using tetrode arrays, which was also revealed after removing latent fluctuations from anesthetized recordings using the same technique (12). Regardless of the underlying reason for this discrepancy between the two above-mentioned studies in the V1 (e.g., layer specificity or the effect or number of samples), our recordings in the PFC provide direct evidence for a nonmonotonic, long-range correlation structure during wakefulness, without the need for removing latent sources of covariance, i.e., without application of GPFA or any other similar tool involving theoretical assumptions like stationarity of responses or the number of latent factors that contribute in driving correlated variability.

Conclusion

Overall, our results suggest that the mesoscopic functional connectivity architecture of vlPFC is fundamentally different compared with early sensory cortices such as V1 or V4. Correlated variability in the vlPFC is spatially nonmonotonic, and a major source of nonmonotonicity is the spatial pattern of correlations between neurons with similar functional properties. A nonmonotonic functional connectivity profile with strong and equivalent local and long-range interactions might reflect the underlying machinery for large-scale coordination of distributed information processing in the PFC.

Experimental Procedures

Electrophysiological Recordings. Extracellular electrophysiological recordings were performed in the inferior convexity of the lateral PFC of two anesthetized and two awake adult, male rhesus macaques (*Macaca mulatta*) by using Utah microelectrode arrays [Blackrock Microsystems (37)]. The array (4×4 mm with a 10×10 electrode configuration and interelectrode distance of 400 μm) was placed 1–2 mm anterior to the bank of the arcuate sulcus and below the ventral bank of the principal sulcus, thus covering a large part of the inferior convexity in the vlPFC (Fig. 1*A*). For the awake experiments, monkeys were implanted with form-specific titanium head posts on the cranium after modeling the skull based on an anatomical MRI scan acquired in a vertical 7T scanner with a 60-cm-diameter bore (Biospec 47/40c; Bruker Medical). The methods for surgical preparation and anesthesia have been described (64–66). All experiments were approved by the local authorities (Regierungspräsidium) and were in full compliance with the guidelines of the European Community (European Union Vendor Declaration 86/609/EEC) for the care and use of laboratory animals.

Data Acquisition and Spike Sorting. Broadband neural signals (0.1–32 kHz in the anesthetized recordings and 0.1–30 kHz in the awake recordings) were recorded by using a Neuralynx (Digital Lynx) data-acquisition system for the anesthetized recordings and Neural Signal Processors (Blackrock Microsystems) for the awake recordings.

In the anesthetized data, to detect spiking activity, we first bandpass-filtered (0.6–5.8 kHz) the broadband raw signal using a minimum-order finite impulse response filter (67) with 65-dB attenuation in the stop bands and <0.002-dB ripple within the pass band. A Gaussian distribution was fit to

randomly selected chunks of the filtered signal to compute the noise variance, and the amplitude threshold for spike detection was set to five times the computed variance. Spike events with interspike intervals less than a refractory period of 0.5 ms were eliminated. Those events that satisfied the threshold and refractory period criteria were kept for spike sorting.

In the awake experiments, broadband data were filtered between 0.3 and 3 kHz by using a second-order Butterworth filter. The amplitude for spike detection was set to five times the median absolute deviation (68). The criterion for rejection of spikes was the same as described above. All of the collected spikes were aligned to the minimum. For spike sorting, 1.5 ms around the peak, i.e., 45 samples, were extracted.

Automatic clustering to detect putative single neurons in both the awake and anesthetized data were achieved by a split and merge expectation–maximization (SMEM) algorithm that fits a mixture of Gaussians to the spike feature data which consisted of the first three principal components. For the anesthetized data, the SMEM algorithm by Ueda et al. (69) was used. Details of the spike-sorting method used in this study have been described using tetrodes (24, 70). For the awake data, the KlustaKwik algorithm (71, 72) was used. The spike-sorting procedure was finalized in both cases through visual inspection by using the program Klusters (73).

Visual Stimulation. In anesthetized recordings, full-field visual stimulation of 640 × 480 resolution with 24-bit true color at 60 Hz for each eye was presented by using a Windows machine equipped with an OpenGL graphics card (Wildcat series; 3DLABS). We used 10-s epochs from a commercially available movie [*Star Wars Episode I*, the Battle of Naboo (74)]. Hardware double buffering was used to provide smooth animation. The experimenter's monitor and the video interface of a fiber-optic stimulus presentation system (Silent Vision; Avotec) were driven by the VGA outputs. The field of view was 30 (horizontal) × 23 (vertical) degrees of visual angle, and the focus was fixed at two diopters. Binocular presentation was possible through two independently positioned plastic, fiber-optic glasses; however, in this study, we used monocular stimulation (either left or right eye). The contact lenses for the eyes had matched diopter with an Avotec projector to focus images on the retina. Positioning was aided by a modified fundus camera (RC250; Carl Zeiss) with an attachment to hold the projector on the same axis of the camera lens. After observing the foveal region, the projector was fixed relative to the animal.

In the awake recordings, the visual stimuli were generated by in-house software written in C/Tcl and used OpenGL implementation. Stimuli were displayed by using a dedicated graphics workstation (TDZ 2000; Intergraph Systems) with a resolution of 1,280 × 1,024 and a 60-Hz refresh rate. An industrial PC with one Pentium CPU (Advantech) running the QNX real-time operating system (QNX Software Systems) controlled the timing of stimulus presentation, digital pulses to the Neuralynx system (anesthetized) or the Blackrock system (awake), and acquisition of images. Eye movements were captured by using an IR camera at 1-kHz sampling rate using the software iView (SensoriMotoric Instruments GmBH). They were monitored online and stored for offline analysis by using both the QNX-based acquisition system and the Blackrock data-acquisition system.

In the anesthetized recordings, neural activity was recorded in 200 trials of repeated stimulus presentation. Each trial consisted of the same 10-s-long movie clip, followed by 10 s of a blank screen (intertrial). In the awake experiments, two monkeys were trained to fixate on a red square of size 0.2° of visual angle subtended on the eye ~45 cm from the monitors and maintain fixation within a window of 1.5–2° of visual angle. The location of the red fixation square was adjusted to the single eye vergence of each individual monkey. After 300 ms of fixation, a moving grating of size 8°, moving at a speed of 12° (monkey H) and 13° (monkey A) per second with a spatial frequency of 0.5 cycles per degree of visual angle and at 100% contrast was presented for 1,000 ms. The gratings encompassed eight different directions of motion, viz. 0°, 45°, 90°, 135°, 180°, 225°, 270°, and 315° (Fig. 1*B*), pseudorandomized within a block of eight trials. After 1,000 ms, a 300-ms stimulus-off period preceded the completion of the trial. The monkeys were given a liquid reward (either water or juice) at the end of the trial, if they maintained fixation within the specified fixation window during the entire duration of the trial. Every successful trial was followed by a 1,000-ms intertrial period. On average, we found 32 ± 5% of all recorded neurons to be visually modulated. The stimuli, although presented through a stereoscope (due to the data being collected on the same day with other experiments requiring dichoptic viewing conditions), were always presented monocularly in the left eye to remain consistent with the monocular stimulation protocol used in the anesthetized recordings. In both anesthetized and awake recordings, to ensure accurate control of stimulus presentation, a photodiode was attached to the experimenter's monitor, permitting the recording of the exact presentation time of every single frame.

In the awake recordings, spontaneous activity datasets were collected on days different from those of the task recordings. The monkeys were allowed to move their eyes freely or have their eyes closed. The recording chamber was sound-resistant and dark. In the anesthetized recordings, spontaneous activity datasets were recorded between periods of visual stimulation. In both the awake and anesthetized recordings of spontaneous activity, the monitors were turned off. The duration of each spontaneous activity dataset was between 40 and 80 min.

Tuning Functions and Signal Correlations. Tuning curves for each detected single unit were computed by averaging the firing rate across trials for each of the eight presented directions of motion. Signal correlations, defined as the correlation coefficient between the tuning curves of a neuronal pair, were also computed (7). In addition to classical tuning curves (direction and orientation selectivity), other types of tunings, such as inverted tunings, for example, have also been reported in the electrophysiological studies of the macaque PFC (75). Because of this variability in the observed tuning properties of detected single units, signal correlation provides a more general measure of response similarity, and therefore it was used to investigate the correlation structure that arises from this functional similarity.

Spike Count Correlations. To compute spike count correlation (r_{sc}) during the anesthetized state, we divided the period of visual stimulation into 10 periods, each being 1,000 ms long, and considered these periods as different successive stimuli. The intertrial period was also binned in the same way. In the awake data, visual stimulation and intertrial periods were 1,000 ms long each, thus being consistent with the anesthetized experiments. We estimated spike counts over 1,000 ms due to the stimulus length used in previous studies of correlated variability. In spontaneous datasets (both anesthetized and awake), the entire length of the recording epoch was split into periods of 1,000 ms that were treated as a trial.

The spike count correlation coefficients were computed similarly to previous studies in primary visual areas (10, 24, 64). First, for each condition (either presentation of each moving grating in awake experiment or a single bin of movie clip in the anesthetized experiment), we normalized the spike counts across all trials by converting them into z scores (10). For each pair, we computed the Pearson's correlation coefficient for the two vectors z_i and z_j as follows:

$$c(r_i, r_j) = E[z_i z_j]. \qquad [1]$$

After computing $c(r_i, r_j)$ for each condition, we averaged across conditions to obtain the correlation value. Equivalently, one can concatenate z scores for all of the conditions in long vectors and find the expectation of their product. To account for possible nonphysiological correlations between detected neurons, which could happen, for example, due to shorts between recording electrodes, a threshold of 5 SDs above the mean correlation value was set, and the outliers were discarded.

Quantification of Spatial Inhomogeneities in Correlated Variability. We quantified the inhomogeneity in the spatial structure of correlated variability across different conditions and states by computing the mean of the absolute rate (i.e., first differential) of correlation changes across lateral distance. To estimate the first differential with respect to distance, we subtracted the mean correlation values of consecutive bins that were significantly different (Wilcoxon rank-sum test, alpha level 0.05). If no significant change between two consecutive bins was observed, the derivative at that point was set to zero.

Curve Fitting Procedures. A two-parameter line ($y = ax + b$) and a three-parameter quadratic function ($y = ax^2 + bx + c$) were fit via a minimization of the least-squared error to the results in Fig. 6 *B* and *D* by using the in-built Curve Fitting Toolbox in MATLAB (Version 2016b). The chosen functions (40) were fit to the mean noise correlation functions, which were weighted by the SEM of each data point as the individual data points spanned varying number of observations.

NEUROSCIENCE

1. Douglas RJ, Martin KAC (2004) Neuronal circuits of the neocortex. *Annu Rev Neurosci* 27:419–451.
2. Harris KD, Mrsic-Flogel TD (2013) Cortical connectivity and sensory coding. *Nature* 503:51–58.
3. Douglas RJ, Martin KAC, Whitteridge D (1989) A canonical microcircuit for neocortex. *Neural Comput* 1:480–488.
4. Douglas RJ, Martin KAC (2007) Mapping the matrix: The ways of neocortex. *Neuron* 56:226–238.
5. Miller KD (2016) Canonical computations of cerebral cortex. *Curr Opin Neurobiol* 37: 75–84.
6. Murray JD, et al. (2014) A hierarchy of intrinsic timescales across primate cortex. *Nat Neurosci* 17:1661–1663.
7. Cohen MR, Kohn A (2011) Measuring and interpreting neuronal correlations. *Nat Neurosci* 14:811–819.
8. Denman DJ, Contreras D (2014) The structure of pairwise correlation in mouse primary visual cortex reveals functional organization in the absence of an orientation map. *Cereb Cortex* 24:2707–2720.
9. Constantinidis C, Goldman-Rakic PS (2002) Correlated discharges among putative pyramidal neurons and interneurons in the primate prefrontal cortex. *J Neurophysiol* 88:3487–3497.
10. Bair W, Zohary E, Newsome WT (2001) Correlated firing in macaque visual area MT: Time scales and relationship to behavior. *J Neurosci* 21:1676–1697.
11. Rothschild G, Nelken I, Mizrahi A (2010) Functional organization and population dynamics in the mouse primary auditory cortex. *Nat Neurosci* 13:353–360.
12. Ecker AS, et al. (2014) State dependence of noise correlations in macaque primary visual cortex. *Neuron* 82:235–248.
13. Sompolinsky H, Yoon H, Kang K, Shamir M (2001) Population coding in neuronal systems with correlated noise. *Phys Rev E Stat Nonlin Soft Matter Phys* 64:051904.
14. Smith MA, Kohn A (2008) Spatial and temporal scales of neuronal correlation in primary visual cortex. *J Neurosci* 28:12591–12603.
15. Schulz DPA, Sahani M, Carandini M (2015) Five key factors determining pairwise correlations in visual cortex. *J Neurophysiol* 114:1022–1033.
16. Chelaru MI, Dragoi V (2016) Negative correlations in visual cortical networks. *Cereb Cortex* 26:246–256.
17. Smith MA, Sommer MA (2013) Spatial and temporal scales of neuronal correlation in visual area V4. *J Neurosci* 33:5422–5432.
18. Constantinidis C, Franowicz MN, Goldman-Rakic PS (2001) Coding specificity in cortical microcircuits: A multiple-electrode analysis of primate prefrontal cortex. *J Neurosci* 21:3646–3655.
19. Amir Y, Harel M, Malach R (1993) Cortical hierarchy reflected in the organization of intrinsic connections in macaque monkey visual cortex. *J Comp Neurol* 334:19–46.
20. Elston GN (2003) Cortex, cognition and the cell: New insights into the pyramidal neuron and prefrontal function. *Cereb Cortex* 13:1124–1138.
21. Lund JS, Yoshioka T, Levitt JB (1993) Comparison of intrinsic connectivity in different areas of macaque monkey cerebral cortex. *Cereb Cortex* 3:148–162.
22. Gochin PM, Miller EK, Gross CG, Gerstein GL (1991) Functional interactions among neurons in inferior temporal cortex of the awake macaque. *Exp Brain Res* 84:505–516.
23. Martin KAC, Roth S, Rusch ES (2014) Superficial layer pyramidal cells communicate heterogeneously between multiple functional domains of cat primary visual cortex. *Nat Commun* 5:5252.
24. Ecker AS, et al. (2010) Decorrelated neuronal firing in cortical microcircuits. *Science* 327:584–587.
25. Rosenbaum R, Smith MA, Kohn A, Rubin JE, Doiron B (2017) The spatial structure of correlated neuronal variability. *Nat Neurosci* 20:107–114.
26. Voges N, Schüz A, Aertsen A, Rotter S (2010) A modeler's view on the spatial structure of intrinsic horizontal connectivity in the neocortex. *Prog Neurobiol* 92:277–292.
27. Angelucci A, et al. (2002) Circuits for local and global signal integration in primary visual cortex. *J Neurosci* 22:8633–8646.
28. Kritzer MF, Goldman-Rakic PS (1995) Intrinsic circuit organization of the major layers and sublayers of the dorsolateral prefrontal cortex in the rhesus monkey. *J Comp Neurol* 359:131–143.
29. Tanigawa H, Wang Q, Fujita I (2005) Organization of horizontal axons in the inferior temporal cortex and primary visual cortex of the macaque monkey. *Cereb Cortex* 15: 1887–1899.
30. Fujita I, Fujita T (1996) Intrinsic connections in the macaque inferior temporal cortex. *J Comp Neurol* 368:467–486.
31. Levitt JB, Lewis DA, Yoshioka T, Lund JS (1993) Topography of pyramidal neuron intrinsic connections in macaque monkey prefrontal cortex (areas 9 and 46). *J Comp Neurol* 338:360–376.
32. Pucak ML, Levitt JB, Lund JS, Lewis DA (1996) Patterns of intrinsic and associational circuitry in monkey prefrontal cortex. *J Comp Neurol* 376:614–630.
33. Schwartz ML, Goldman-Rakic PS (1984) Callosal and intrahemispheric connectivity of the prefrontal association cortex in rhesus monkey: Relation between intraparietal and principal sulcal cortex. *J Comp Neurol* 226:403–420.
34. Yoshioka T, Blasdel GG, Levitt JB, Lund JS (1996) Relation between patterns of intrinsic lateral connectivity, ocular dominance, and cytochrome oxidase-reactive regions in macaque monkey striate cortex. *Cereb Cortex* 6:297–310.
35. Goldman-Rakic PS, Schwartz ML (1982) Interdigitation of contralateral and ipsilateral columnar projections to frontal association cortex in primates. *Science* 216:755–757.
36. Melchitzky DS, González-Burgos G, Barrionuevo G, Lewis DA (2001) Synaptic targets of the intrinsic axon collaterals of supragranular pyramidal neurons in monkey prefrontal cortex. *J Comp Neurol* 430:209–221.
37. Maynard EM, Nordhausen CT, Normann RA (1997) The Utah intracortical electrode array: A recording structure for potential brain-computer interfaces. *Electroencephalogr Clin Neurophysiol* 102:228–239.
38. Paradiso MA, Meshi D, Pisarcik J, Levine S (2012) Eye movements reset visual perception. *J Vis* 12:11.
39. Goldman-Rakic PS (1995) Cellular basis of working memory. *Neuron* 14:477–485.
40. Mandel J (1981) Fitting curves and surfaces with monotonic and non-monotonic four parameter equations. *J Res Natl Bur Stand* 86:1.
41. Hubel DH, Wiesel TN, Stryker MP (1978) Anatomical demonstration of orientation columns in macaque monkey. *J Comp Neurol* 177:361–380.
42. Giguere M, Goldman-Rakic PS (1988) Mediodorsal nucleus: Areal, laminar, and tangential distribution of afferents and efferents in the frontal lobe of rhesus monkeys. *J Comp Neurol* 277:195–213.
43. Eblen F, Graybiel AM (1995) Highly restricted origin of prefrontal cortical inputs to striosomes in the macaque monkey. *J Neurosci* 15:5999–6013.
44. Miller EK, Cohen JD (2001) An integrative theory of prefrontal cortex function. *Annu Rev Neurosci* 24:167–202.
45. Modha DS, Singh R (2010) Network architecture of the long-distance pathways in the macaque brain. *Proc Natl Acad Sci USA* 107:13485–13490.
46. Chen J, Hasson U, Honey CJ (2015) Processing timescales as an organizing principle for primate cortex. *Neuron* 88:244–246.
47. Chaudhuri R, Knoblauch K, Gariel M-A, Kennedy H, Wang X-J (2015) A large-scale circuit mechanism for hierarchical dynamical processing in the primate cortex. *Neuron* 88:419–431.
48. Chaudhuri R, Bernacchia A, Wang X-J (2014) A diversity of localized timescales in network activity. *elife* 3:e01239.
49. Timme N, et al. (2014) Multiplex networks of cortical and hippocampal neurons revealed at different timescales. *PLoS One* 9:e115764.
50. Bullmore E, Sporns O (2009) Complex brain networks: Graph theoretical analysis of structural and functional systems. *Nat Rev Neurosci* 10:186–198.
51. Latora V, Marchiori M (2003) Economic small-world behavior in weighted networks. *Eur Phys J B* 32:249–263.
52. Latora V, Marchiori M (2001) Efficient behavior of small-world networks. *Phys Rev Lett* 87:198701.
53. Masse NY, Hodnefield JM, Freedman DJ (2017) Mnemonic encoding and cortical organization in parietal and prefrontal cortices. *J Neurosci* 37:6098–6112.
54. Kiani R, et al. (2015) Natural grouping of neural responses reveals spatially segregated clusters in prearcuate cortex. *Neuron* 85:1359–1373.
55. Markowitz DA, Curtis CE, Pesaran B (2015) Multiple component networks support working memory in prefrontal cortex. *Proc Natl Acad Sci USA* 112:11084–11089.
56. Tsujimoto S, Genovesio A, Wise SP (2008) Transient neuronal correlations underlying goal selection and maintenance in prefrontal cortex. *Cereb Cortex* 18:2748–2761.
57. Sakurai Y, Takahashi S (2006) Dynamic synchrony of firing in the monkey prefrontal cortex during working-memory tasks. *J Neurosci* 26:10141–10153.
58. Leavitt ML, Pieper F, Sachs A, Joober R, Martinez-Trujillo JC (2013) Structure of spike count correlations reveals functional interactions between neurons in dorsolateral prefrontal cortex area 8a of behaving primates. *PLoS One* 8:e61503.
59. Hussar CR, Pasternak T (2009) Flexibility of sensory representations in prefrontal cortex depends on cell type. *Neuron* 64:730–743.
60. Hansen BJ, Chelaru MI, Dragoi V (2012) Correlated variability in laminar cortical circuits. *Neuron* 76:590–602.
61. Smith MA, Jia X, Zandvakili A, Kohn A (2013) Laminar dependence of neuronal correlations in visual cortex. *J Neurophysiol* 109:940–947.
62. Hahn TTG, Sakmann B, Mehta MR (2007) Differential responses of hippocampal subfields to cortical up-down states. *Proc Natl Acad Sci USA* 104:5169–5174.
63. Petersen CCH, Hahn TTG, Mehta M, Grinvald A, Sakmann B (2003) Interaction of sensory responses with spontaneous depolarization in layer 2/3 barrel cortex. *Proc Natl Acad Sci USA* 100:13638–13643.
64. Belitski A, et al. (2008) Low-frequency local field potentials and spikes in primary visual cortex convey independent visual information. *J Neurosci* 28:5696–5709.
65. Logothetis NK, Guggenberger H, Peled S, Pauls J (1999) Functional imaging of the monkey brain. *Nat Neurosci* 2:555–562.
66. Logothetis N, Merkle H, Augath M, Trinath T, Ugurbil K (2002) Ultra high-resolution fMRI in monkeys with implanted RF coils. *Neuron* 35:227–242.
67. Rabiner LR, McClellan JH, Parks TW (1975) FIR digital filter design techniques using weighted Chebyshev approximation. *Proc IEEE* 63:595–610.
68. Quiroga RQ, Nadasdy Z, Ben-Shaul Y (2004) Unsupervised spike detection and sorting with wavelets and superparamagnetic clustering. *Neural Comput* 16:1661–1687.
69. Ueda N, Nakano R, Ghahramani Z, Hinton GE (2000) SMEM algorithm for mixture models. *Neural Comput* 12:2109–2128.
70. Tolias AS, et al. (2007) Recording chronically from the same neurons in awake, behaving primates. *J Neurophysiol* 98:3780–3790.
71. Kadir SN, Goodman DFM, Harris KD (2014) High-dimensional cluster analysis with the masked EM algorithm. *Neural Comput* 26:2379–2394.
72. Harris KD, Henze DA, Csicsvari J, Hirase H, Buzsáki G (2000) Accuracy of tetrode spike separation as determined by simultaneous intracellular and extracellular measurements. *J Neurophysiol* 84:401–414.
73. Hazan L, Zugaro M, Buzsáki G (2006) Klusters, NeuroScope, NDManager: A free software suite for neurophysiological data processing and visualization. *J Neurosci Methods* 155:207–216.
74. Lucas G (1999) *Star Wars: Episode I—The Phantom Menace* [motion picture], director Lucas G (Lucasfilm).
75. Zhou X, Katsuki F, Qi X-L, Constantinidis C (2012) Neurons with inverted tuning during the delay periods of working memory tasks in the dorsal prefrontal and posterior parietal cortex. *J Neurophysiol* 108:31–38.